The Astrophysical Journal Letters, 946:L36 (9pp), 2023 April 1 https://doi.org/10.3847/2041-8213/acbd4f

A 2:1 Mean-motion Resonance Super-Jovian Pair Revealed by TESS, FEROS, and HARPS*

Vladimir Bozhilov[1], Desislava Antonova[1], Melissa J. Hobson[2,3], Rafael Brahm[3,4,5], Andrés Jordán[3,4,5], Thomas Henning[2], Jan Eberhardt[2], Felipe I. Rojas[3,6], Konstantin Batygin[7], Pascal Torres-Miranda[3,6], Keivan G. Stassun[8], Sarah C. Millholland[9], Denitza Stoeva[1], Milen Minev[1,10], Nestor Espinoza[11], George R. Ricker[12], David W. Latham[13], Diana Dragomir[14], Michelle Kunimoto[12], Jon M. Jenkins[15], Eric B. Ting[15], Sara Seager[12,16,17], Joshua N. Winn[18], Jesus Noel Villasenor[12], Luke G. Bouma[19], Jennifer Medina[11], and Trifon Trifonov[1,2]

[1] Department of Astronomy, Faculty of Physics, Sofia University "St Kliment Ohridski," 5 James Bourchier Blvd., BG-1164 Sofia, Bulgaria
vbozhilov@phys.uni-sofia.bg
[2] Max-Planck-Institut für Astronomie, Königstuhl 17, D-69117 Heidelberg, Germany
[3] Millennium Institute for Astrophysics, Chile
[4] Facultad de Ingeniera y Ciencias, Universidad Adolfo Ibáñez, Av. Diagonal las Torres 2640, Peñalolén, Santiago, Chile
[5] Data Observatory Foundation, Chile
[6] Instituto de Astrofísica, Facultad de Física, Pontificia Universidad Católica de Chile, Chile
[7] Division of Geological and Planetary Sciences, California Institute of Technology, Pasadena, CA 91125, USA
[8] Department of Physics and Astronomy, Vanderbilt University, Nashville, TN 37235, USA
[9] MIT Kavli Institute for Astrophysics and Space Research, Massachusetts Institute of Technology, Cambridge, MA 02139, USA
[10] Institute of Astronomy and National Astronomical Observatory, Bulgarian Academy of Sciences, 72 Tsarigradsko shosse Blvd., 1784 Sofia, Bulgaria
[11] Space Telescope Science Institute, 3700 San Martin Drive, Baltimore, MD 21218, USA
[12] Department of Physics and Kavli Institute for Astrophysics and Space Research, Massachusetts Institute of Technology, Cambridge, MA 02139, USA
[13] Center for Astrophysics, Harvard & Smithsonian, 60 Garden St., Cambridge, MA 02138, USA
[14] Department of Physics and Astronomy, University of New Mexico, Albuquerque, NM, USA
[15] NASA Ames Research Center, Moffett Field, CA 94035, USA
[16] Department of Earth, Atmospheric and Planetary Sciences, Massachusetts Institute of Technology, Cambridge, MA 02139, USA
[17] Department of Aeronautics and Astronautics, MIT, 77 Massachusetts Avenue, Cambridge, MA 02139, USA
[18] Department of Astrophysical Sciences, Princeton University, NJ 08544, USA
[19] Cahill Center for Astrophysics, California Institute of Technology, Pasadena, CA 91125, USA
Received 2023 January 19; revised 2023 February 13; accepted 2023 February 20; published 2023 March 29

Abstract

We report the discovery of a super-Jovian 2:1 mean-motion resonance (MMR) pair around the G-type star TIC 279401253, whose dynamical architecture is a prospective benchmark for planet formation and orbital evolution analysis. The system was discovered thanks to a single-transit event recorded by the Transiting Exoplanet Survey Satellite mission, which pointed to a Jupiter-sized companion with poorly constrained orbital parameters. We began ground-based precise radial velocity (RV) monitoring with HARPS and FEROS within the Warm gIaNts with tEss survey to constrain the transiting body's period, mass, and eccentricity. The RV measurements revealed not one but two massive planets with periods of $76.80^{+0.06}_{-0.06}$ and $155.3^{+0.7}_{-0.7}$ days, respectively. A combined analysis of transit and RV data yields an inner transiting planet with a mass of $6.14^{+0.39}_{-0.42}$ $M_{\rm Jup}$ and a radius of $1.00^{+0.04}_{-0.04}$ $R_{\rm Jup}$, and an outer planet with a minimum mass of $8.02^{+0.18}_{-0.18}$ $M_{\rm Jup}$, indicating a massive giant pair. A detailed dynamical analysis of the system reveals that the planets are locked in a strong first-order, eccentricity-type 2:1 MMR, which makes TIC 279401253 one of the rare examples of truly resonant architectures supporting disk-induced planet migration. The bright host star, $V \approx 11.9$ mag, the relatively short orbital period ($P_{\rm b} = 76.80^{+0.06}_{-0.06}$ days), and pronounced eccentricity ($e = 0.448^{+0.028}_{-0.029}$) make the transiting planet a valuable target for atmospheric investigation with the James Webb Space Telescope and ground-based extremely large telescopes.

Unified Astronomy Thesaurus concepts: Radial velocity (1332); Transit photometry (1709); Exoplanets (498); Exoplanet systems (484); Exoplanet dynamics (490); Exoplanet evolution (491); Exoplanet migration (2205); Exoplanet astronomy (486); Extrasolar gaseous planets (2172)

1. Introduction

The number of known exoplanets discovered by different surveys up to 2022 December is more than 5200, including around 850 multiple-planet systems.[20] The majority of these exoplanets have been detected using the transit technique, primarily thanks to the highly successful NASA Kepler space

* Based on observations collected at the European Organization for Astronomical Research in the Southern Hemisphere under ESO programmes 105.20GX.001, 108.22A8.001, 110.23YQ.001, and MPG programmes 0106.A-9014, 0107.A-9003, 0108.A-9003, 0109.A-9003, 0110.A-9011.

[20] http://exoplanet.eu/catalog/

telescope (Borucki et al. 2010), and the ongoing Transiting Exoplanet Survey Satellite (TESS; Ricker et al. 2015) mission. However, the transit signals alone do not reveal the planetary mass and orbital eccentricity. A better picture of the distribution of the planetary radii, dynamical masses, bulk densities, and orbital geometry is fundamentally important for studying exoplanet composition, evolution, and overall formation. Therefore, validating and characterizing orbital and physical parameters of transiting planets with precise radial velocity (RV) data is fundamentally important to link observations with theory.

The TESS survey has revealed many well-characterized exoplanet systems for which both mass and radius have been determined observationally. Indeed, the relatively small TESS telescope is the main instrument for the discovery of transiting exoplanets around relatively bright stars, which allows them to be confirmed with ground-based precise RV measurements. A major role in the global efforts to characterize TESS exoplanets is played by the Warm gIaNts with tEss (WINE) survey, which aims for the validation of warm (with periods ranging between 10 days $< P <$ 300 days) Jovian gas giants by inspecting the TESS Full Frame Images (FFI) data. Prospective targets are followed by an extensive RV monitoring with the FEROS[21] and the HARPS[22] precise RV spectrographs. The WINE survey has been highly successful, having detected and characterized many giant planets (see, e.g., Brahm et al. 2020; Espinoza et al. 2020; Jordán et al. 2020; Schlecker et al. 2020; Trifonov et al. 2021b, among many more).

In this paper, we report the discovery of a warm massive exoplanet pair around a G-dwarf star, which has been uncovered within the WINE-TESS follow-up survey, based on RVs obtained with HARPS and FEROS. We present the TIC 279401253 two-planet system, which exhibits a significant single transiting event detected in TESS, consistent with a Jovian-sized planet. However, the acquired RVs of the TIC 279401253 system undoubtedly reveal a strongly interacting warm giant-mass pair of planets locked in a 2:1 mean-motion resonance (MMR) commensurability. The detection and observational characterization of warm Jovian planets in 2:1 MMR is still a rare event, despite its importance for constraining planet migration.

The observatinal data is presented in Section 2. We use this data to detect and characterize the warm pair of planets that orbit around TIC 279401253. We present our estimates of the stellar parameters of TIC 279401253 in Section 3, along with the planetary orbital analysis performed jointly with the acquired Doppler data and TESS photometry. In Section 3, we also provide our results from an analysis on the dynamical architecture and long-term stability of the TIC 279401253 system. Finally, in Section 4, we present a brief summary and our conclusions.

2. Data

2.1. TESS

TIC 279401253 was visited by TESS during Sectors 4 and 31. Our team identified a single-transit event in the light curves extracted from the TESS 10 minute FFIs of Sector 31, using the TESSERACT[23] pipeline (F. I. Rojas et al. 2023, in preparation). The left panel of Figure 1 shows the target pixel file (TPF) image of TIC 279401253 constructed from the TESS FFI image frames and Gaia DR3 data (Gaia Collaboration et al. 2021). The right panel of Figure 1 shows the detrended TESSERACT FFI light curve centered around the transit event, together with a transit model fit to the data. We did not identify bright contaminators in the FFI aperture (red continuous contour); thus we concluded that the transit signals are indeed coming from TIC 279401253 and not from neighboring stars.

The 2 minute cadence light curves are retrieved from the Mikulski Archive for Space Telescopes.[24] 24 Simple aperture photometry (SAP) and systematics-corrected Pre-search Data Conditioning photometry (PDC; Stumpe et al. 2012; Smith et al. 2012) are provieded by the The Science Processing Operations Center (SPOC; Jenkins et al. 2016). The PDCSAP light curves are corrected for instrumental systematics originating from pointing drifts, focus changes, etc., and for contamination from nearby stars.

2.2. RV Data

After the detection of the TESS transit, we initiated a Doppler follow-up campaign by obtaining precise RV data with the FEROS and HARPS spectrographs. We obtained 19 spectra of TIC 279401253 with FEROS between 2021 February and 2022 October, and 14 spectra with HARPS between 2021 September and 2022 October. With both instruments, we recorded stellar spectra in conjunction with a simultaneous ThAr lamp used for wavelength calibration. The exposure times were set to 1800 s, yielding an average signal-to-noise ratio per spectral resolution element of 76 for FEROS, and 34 for HARPS, respectively.

The FEROS spectra were reduced, extracted, and analyzed with the `ceres` pipeline (Brahm et al. 2017a). For the HARPS spectra, we retrieved precise RV measurements derived by the ESO-DRS pipeline. Both `ceres` and ESO-DRS use a spectrum cross-correlation function (CCF) method with a weighted binary mask (Pepe et al. 2002). With `ceres`, we measure FEROS RVs and bisector span measurements with a mean uncertainty of $\hat{\sigma}_{\rm FEROS} = 8.2\ {\rm m\,s^{-1}}$. The DRS pipeline also provides the CCF's FWHM and the Bisector Inverse Slope span (BIS-span) measurements, which are valuable stellar activity indicators (Queloz et al. 2001). The mean RV uncertainty of ESO-DRS is $\hat{\sigma}_{\rm HARPS} = 2.9\ {\rm m\,s^{-1}}$. When combined in common mean RV offset, the Doppler velocities show very large end-to-end periodic RV amplitude of $\sim$880 $\rm m\,s^{-1}$, a suggesting a massive substellar companion (or companions). We did not detect any significant periodicity in the FEROS and HARPS activity data. The obtained FEROS RVs are presented in Table A1, and the precise HARPS-DRS RVs and activity index data are tabulated in Table A2.

3. Analysis and Results

3.1. Stellar Parameters

TIC 279401253 is a G-type star visible in the Southern Hemisphere. The star is at a distance of about $287.1^{+1.9}_{-1.9}$ pc from the Sun and has an apparent magnitude of $V = 11.9$ mag. The atmospheric and physical parameters were obtained using

[21] The Fiber-fed Extended Range Optical Spectrograph (FEROS; Kaufer et al. 1999).
[22] High Accuracy Radial velocity Planet Searcher at the ESO La Silla 3.6 m telescope (HARPS; Mayor et al. 2003).
[23] https://github.com/astrofelipe/tesseract
[24] http://mast.stsci.edu/portal/Mashup/Clients/Mast/Portal.html

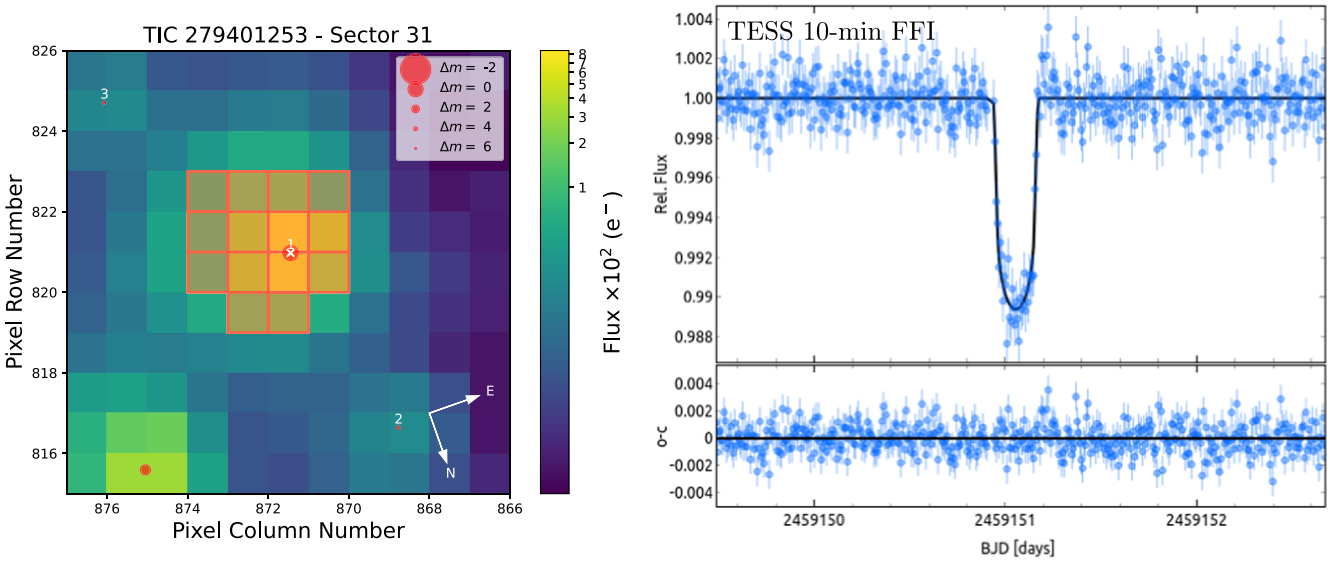

Figure 1. The left panel shows the TPF image of TIC 279401253 for TESS Sector 31. The red pixels indicate the combined aperture used to compute the photometry. The Gaia targets are shown with red circles, whose size is coded by their G magnitude. The right panel shows the TESSERACT 10 minute FFI light curve of TIC 279401253 around the single-transit event recorded in Sector 31. The model curve shows a transit model to the data, and the small bottom panel shows the residuals of the fit.

three coadded HARPS spectra and the ZASPE code (Brahm et al. 2017b). For TIC 279401253 we obtain an effective temperature of $T_{\rm eff} = 5951 \pm 80$ K, a metallicity of [Fe/H] $= +0.20 \pm 0.05$, and a projected rotational velocity of $v \sin i = 5.0 \pm 0.5$ km s^{-1}. Further, we derive stellar physical parameters using the PARSEC stellar isochrones (Bressan et al. 2012), following the recipe in Brahm et al. (2018) in conjunction with the Gaia parallaxes, and the public broadband photometry (G, G_{BP}, G_{RP}, J, H, K). We derive a stellar mass of $M_\star = 1.13^{+0.02}_{-0.03}$ $M_\odot$ and a stellar radius of $R_\star = 1.06 \pm 0.01$ $R_\odot$. We list the remaining atmospheric and physical parameters in Table 1.

3.2. Orbital Analysis

For the transit, RV, and joint RV-transit analyses, we use the Exo-Striker exoplanet toolbox[25] (Trifonov 2019). Exo-Striker allows for the use of multiple-Keplerian or self-consistent N-body dynamical models. During the course of our analysis, though, we concluded that a single-transit event and the relatively sparse RV data led to strong degeneracies in the N-body model. Therefore, in this work, we only make use of the Keplerian model. The parameters in our transit model are the period P, eccentricity e, argument of periastron ω, inclination i, time of inferior transit conjunction t_0, and the planetary semimajor axis $a/R_\star$, and radius $r/R_\star$ (in relative stellar units), respectively. Additionally, we use quadratic limb darkening parameters for modeling the light curve. The parameters in our RV model are the RV semiamplitude K, orbital period P, eccentricity e, argument of periastron ω, and mean anomaly M_0. All these parameters are valid for BJD = 2,459,151.0, which was deliberately chosen slightly before the epoch of the TESS midtransit event. Additional fitting parameters in our RV modeling of TIC 279401253 were the FEROS and HARPS RV data offsets and variance (i.e., RV jitter, Baluev 2009).

[25] https://github.com/3fon3fonov/exostriker

Table 1
Stellar Parameters of TIC 279401253 and Their 1σ Uncertainties Derived Using ZASPE Analyses of HARPS Spectra, Gaia DR3 Parallax, Broadband Photometry, and PARSEC Models

Parameter	
Distance (1) (pc)	$287.1^{+1.9}_{-1.9}$
Mass ($M_\odot$)	$1.13^{+0.02}_{-0.03}$
Radius ($R_\odot$)	$1.06^{+0.01}_{-0.01}$
Luminosity ($L_\odot$)	$1.25^{+0.05}_{-0.04}$
Age (Gyr)	$1.2^{+1.0}_{-0.8}$
A_V (mag)	$0.09^{+0.06}_{-0.05}$
$T_{\rm eff}$ (K)	5951 ± 80
$\log g$ (cm s^{-2})	4.438 ± 0.015
[Fe/H]	0.20 ± 0.05
$v \cdot \sin(i)$ (km s^{-1})	5.0 ± 0.5

References. (1) Gaia Collaboration et al. (2021).

For deriving the best-fit orbital parameters, we adopted a maximum likelihood estimator (MLE) scheme, which optimizes the parameters via the Nelder–Mead simplex algorithm (Nelder & Mead 1965), followed by a Levenberg–Marquardt (LM) algorithm (Press et al. 1992). These best-fit estimates and the LM covariance matrix confidence intervals serve as prior knowledge for our more detailed Bayesian posterior analysis of the orbital parameters. The latter was constructed using the dynesty sampler (Speagle 2020), which utilizes a nested sampling scheme (NS; Skilling 2004).

3.2.1. TESS Analysis

Since the TESS light curve contains of only a single-transit event, no meaningful period estimate could be derived. However, the transit shape depends on the orbital inclination, the planet radius, $r_p/R_\star$, and the ratio of the semimajor axis of the planetary orbit to the stellar radius, $a_p/R_\star$. The latter is related to Kepler's third law, from which we could obtain a crude estimate of the orbital period (e.g., Sandford et al. 2019).

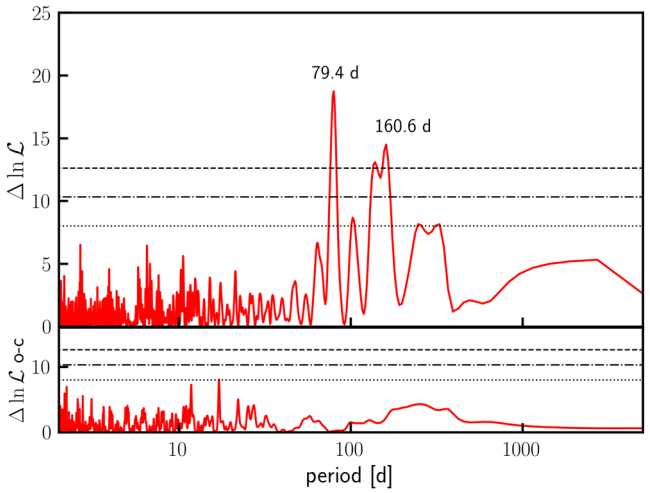

Figure 2. The MLP power spectrum of the combined FEROS and HARPS Doppler measurements of TIC 279401253. Horizontal lines reflect the $\Delta \ln L$ values, which correspond to 0.1%, 1%, and 10% false alarm probabilities (from top to bottom). Two significant periods are detected: one near 79.4 days and the other near 160.6 days. The bottom panel shows the residuals of our two-planet best-fit model (see Table 2), no significant peaks are observed.

Assuming a circular orbit, we fit the TESS light curve with a Keplerian model, and we extract a midtransit time $t_0 = 2{,}459{,}151.054^{+0.001}_{-0.001}$ BJD, an inclination $i = 89.8^{+0.1}_{-0.1}$ deg, a companion radius $R_b = 1.00^{+0.03}_{-0.03}$ $R_{\rm Jup}$, and an orbital period $P = 82.9^{+23.1}_{-22.2}$ days. Based on these estimates, we initiated an RV follow-up within the WINE survey to confirm and characterize the planetary companion.

3.2.2. RV-only Analysis

The precise Doppler data of TIC 279401253 exhibited strong periodicity, which could be attributed to a planetary companion. We performed a period search analysis by computing a maximum likelihood periodogram (MLP; Baluev 2008) to the combined HARPS and FEROS data set. The MLP fits a sine curve to the RV data for a given frequency grid and optimizes the semiamplitude, phase, RV offset, and RV jitter parameters of FEROS and HAPRS. The resulting $\Delta \ln \mathcal{L}$ power spectrum is shown on Figure 2. We detected two significant periods, one near 79.4 days and the other near 160.6 days.

A single Keplerian with a base period of 79.4 days did not lead to an adequate fit to the RV data. An MLP to the residuals confirmed the ∼160 days significant period. The combined RV data are consistent with two strong periodic signals in the 2:1 period ratio commensurability. We found that a two-planet Keplerian model presented an excellent RV solution with no significant periodicities left in the residuals. Our MLE best-fit suggests planetary periods of $P_{\rm b} = 77.21 \pm 0.07$ days, and $P_{\rm c} = 154.5 \pm 0.4$ days, RV semiamplitudes of $K_{\rm b} = 340.7 \pm 12.1$ m s^{-1}, and $K_{\rm c} = 265.6 \pm 4.1$ m s^{-1}, and eccentricities of $e_{\rm b} = 0.46 \pm 0.02$ day, and $e_{\rm c} = 0.18 \pm 0.04$ day, for the inner and the outer planet, respectively. We derived minimum planetary masses of $m_b \sin(i) \sim 6.9 M_{\rm jup}$, and $m_c \sin(i) \sim 7.5$ $M_{\rm jup}$, respectively.

3.2.3. RV-TESS Joint Analysis

We use the individual transit and RV parameters' MLE estimates to define our prior ranges. Then we run a joint MLE fit and NS global parameter posterior analysis. The single-transit event, together with the evidence of two similar Jovian-mass planets, poses the question, which planet actually transits? We tested both possibilities and could construct a consistent joint fit only when the TESS transit event is related to the inner planet, TIC 279401253 b. Therefore, our work only discusses fits with TIC 279401253 b being the transiting planet.

We performed an NS run, which allowed us to efficiently explore the parameter space of orbital elements and study the probability distribution of the posteriors. We ran 100 "live-points" per fitted parameter using the "Dynamic" NS scheme, focused on 100% posterior convergence instead of log-evidence (see Speagle 2020, for details). The final adopted parameter priors, posteriors, and best-fit solution are listed in Table 2. The right panel of Figure 1 shows the transit joint model counterpart to the TESS data. Figure 3 shows the RV data together with the best-fit Doppler joint model of TIC 279401253 constrained by the single TESS transit event. The middle and right bottom panels of Figure 3 show a phase-folded representation of the RV signals of TIC 279401253 b and c, respectively. There are no significant periods left in the residuals of this fit, as can be seen from the bottom panel of Figure 2. The final posterior probability distributions are shown in Figure A1. We note that our analysis is not strictly coplanar, as can be seen from Table 2. While we fit the inclination of the transiting planet, the inclination of the outer planet remains fixed at 90° (and $\Delta\Omega = 0°$). Therefore, our posterior distribution is consistent with a nearly coplanar edge-on system, which is a plausible outcome of the system architecture. The real mutual inclination, however, could be larger and is not possible to be revealed given the available data. Future additional transit and RV data in conjunction with photodynamical modeling could reveal the system architecture better. Furthermore, RV measurements during the transit events could measure the magnitude of the Rossiter–Mclaughlin effect, providing a valuable insight into the spin–orbit alignment of the planet's orbit with respect to the stellar rotation, thus offering a powerful tool to study its formation and subsequent orbital evolution. However, a more precise constraint on the transit timing would be required to make these observations feasible.

Our final estimates for TIC 279401253 b and c lead to planetary orbital periods of $P_b = 76.80^{+0.06}_{-0.06}$ days, and $P_c = 155.3^{+0.7}_{-0.7}$ days, eccentricities of $e_b = 0.448^{+0.029}_{-0.028}$ and $e_c = 0.254^{+0.042}_{-0.036}$. We measured a dynamical mass of $m_b = 6.14^{+0.39}_{-0.42}$ $M_{\rm jup}$, and a minimum mass of $m_c \sin(i) = 8.02^{+0.18}_{-0.18}$ $M_{\rm jup}$, for the inner and outer planet, respectively.

3.3. TIC 279401253: A 2:1 MMR Exoplanet System

The companion periods, eccentricities, and masses in the TIC 279401253 system point to a strongly interacting planet pair, which is likely involved in a 2:1 MMR. Therefore, we performed detailed numerical orbital evolution simulations to test this possibility and study the system's dynamical architecture. We use a custom version of the SYMBA symplectic N-body algorithm (Duncan et al. 1998) integrated in the `Exo-Striker` toolbox, which directly adopts and integrates the Jacobi orbital elements from the posterior orbital analysis. We tested the stability of the TIC 279401253 system up to 1 Myr with a small time step of 0.2 days for 5000 randomly chosen samples from the joint transit+RV orbital parameter posteriors. For each integrated sample, we

Table 2
Nested Sampling Priors, Posteriors, and the Optimum $-\ln \mathcal{L}$ Orbital Parameters of the Two-planet System TIC 279401253 Derived by Joint Modeling of TESS Data, and RVs from FEROS and HARPS

	Median and σ		Max. $-\ln \mathcal{L}$		Adopted Priors	
Parameter	Planet b	Planet c	Planet b	Planet c	Planet b	Planet c
K (m s^{-1})	$302.0^{+22.6}_{-21.0}$	$286.9^{+5.9}_{-5.7}$	314.6	287.5	$\mathcal{U}(200.0, 400.0)$	$\mathcal{U}(200.0, 400.0)$
P (days)	$76.80^{+0.06}_{-0.06}$	$155.3^{+0.7}_{-0.7}$	76.82	155.25	$\mathcal{U}(74.0, 80.0)$	$\mathcal{U}(150.0, 160.0)$
e	$0.448^{+0.029}_{-0.028}$	$0.254^{+0.042}_{-0.036}$	0.454	0.215	$\mathcal{N}(0.0, 0.2)$	$\mathcal{N}(0.0, 0.2)$
ω (deg)	$137.6^{+6.1}_{-6.7}$	$120.9^{+7.9}_{-8.1}$	139.5	128.2	$\mathcal{U}(0.0, 360.0)$	$\mathcal{U}(0.0, 360.0)$
t_0–2,459,000 (BJD)	$151.055^{+0.001}_{-0.001}$	⋯	151.055	⋯	$\mathcal{U}(151.0, 151.1)$	...
M_0 (deg)	⋯	$190.7^{+9.6}_{-10.2}$	⋯	182.4	⋯	$\mathcal{U}(0.0, 360.0)$
i (deg)	$89.59^{+0.27}_{-0.25}$	90.0	89.56	90.0	$\mathcal{N}(90.0, 0.5)$	(fixed)
$a_p/R_\star$	$71.9^{+5.2}_{-4.4}$	⋯	75.2⋯	...	$\mathcal{U}(65.00, 85.00)$	...
$r_p/R_\star$	$0.094^{+0.003}_{-0.004}$	⋯	0.097⋯	...	$\mathcal{U}(0.08, 0.12)$	...
a (au)	$0.369^{+0.003}_{-0.003}$	$0.591^{+0.005}_{-0.006}$	0.369	0.591	(derived)	(derived)
m ($M_{\rm jup}$)	$6.14^{+0.39}_{-0.42}$	$8.02^{+0.18}_{-0.18}$	6.38	8.12	(derived)	(derived)
R ($R_{\rm jup}$)	$1.00^{+0.04}_{-0.04}$	⋯	1.03	⋯	(derived)	...
RV$_{\rm off.}$ FEROS (m s^{-1})	$14576.1^{+6.5}_{-6.5}$	⋯	14579.8	⋯	$\mathcal{U}(14000.0, 15000.0)$	...
RV$_{\rm off.}$ HARPS (m s^{-1})	$14595.3^{+5.9}_{-5.6}$	⋯	14594.1	⋯	$\mathcal{U}(14000.0, 15000.0))$	...
RV$_{\rm jit.}$ FEROS (m s^{-1})	$19.9^{+4.9}_{-3.8}$	⋯	17.6	⋯	$\mathcal{J}(0.0, 50.0)$	...
RV$_{\rm jit.}$ HARPS (m s^{-1})	$9.9^{+3.9}_{-2.5}$	⋯	9.2	⋯	$\mathcal{J}(0.0, 50.0)$	...
Tran.$_{\rm off.}$ TESS–S31 (ppm)	174^{+32}_{-32}	⋯	173	⋯	$\mathcal{U}(-1000.0, 1000.0)$	...
Tran.$_{\rm jit.}$ TESS–S31 (ppm)	30^{+35}_{-16}	⋯	37	⋯	$\mathcal{J}(0.0, 100)$	...
LD-quad.$_1$ TESS–S31	$0.36^{+0.19}_{-0.19}$	⋯	0.44	⋯	$\mathcal{U}(0.0, 1.0)$	...
LD-quad.$_2$ TESS–S31	$0.52^{+0.32}_{-0.34}$	⋯	0.65	⋯	$\mathcal{U}(0.0, 1.0)$	...

Note. The orbital elements are in the Jacobi frame and are valid for epoch BJD = 2,459,151.0. The adopted priors are listed in the rightmost columns and their meanings are $\mathcal{U}$—Uniform, $\mathcal{N}$—Gaussian, and $\mathcal{J}$—Jeffrey's (log-uniform) priors. The derived planetary posterior parameters of a, m, and R are calculated taking into account the stellar parameter uncertainties.

automatically monitored the evolution of the planetary semimajor axes, eccentricities, secular apsidal angle $\Delta\omega = \omega_{\rm b} - \omega_{\rm c}$, and first-order 2:1 MMR angles $\theta_1 = \lambda_{\rm b} - 2\lambda_{\rm c} + \omega_{\rm b}$, $\theta_2 = \lambda_{\rm b} - 2\lambda_{\rm c} + \omega_{\rm c}$, where $\lambda_{\rm b,c} = M_{\rm b,c} + \omega_{\rm b,c}$ is the mean longitude of planet b and c, respectively (see, e.g., Lee 2004).

We found that 73.4% of the examined 5000 samples are stable for 1 Myr, whereas the best-fit, for which we ran a longer simulation, is stable for 10 Myr. We found that the stable configurations exhibit common dynamical behavior with the system locked in the 2:1 MMR. Figure 4 shows an example of a 500 yr extent of the orbital evolution simulation started from the best-fit (i.e., maximum $-\ln \mathcal{L}$; see Table 2). We show the evolution of the mutual period ratio $P_{\rm rat.}$, and of the eccentricities $e_{\rm b}$ and $e_{\rm c}$. The TIC 279401253 system is stable and osculates in the eccentricities and in the 2:1 period ratio. The apsidal alignment argument $\Delta\omega$ librates around 0° with semiamplitude of ∼65°, whereas the characteristic 2:1 MMR angles, θ_1 and θ_2, librate around 0° with semiamplitudes respectively of ∼30° and ∼55°. Therefore, the massive planetary pair is locked in a 2:1 MMR with a short secular timescale of the order of ∼45 yr.

We observed a similar dynamical picture when we studied the stable posterior probability distribution. We found that 90% of the stable samples are locked in 2:1 MMR with $\Delta\omega$, θ_1, and θ_2 librating around 0°, with median semiamplitudes of 62.3°, 31.7°, and 54.8°, respectively.

3.4. Transit Predictions

As we discussed in Section 3.3, the 2:1 MMR system is dynamically active for a short time. Therefore, we expect strong transit timing variations (TTVs), which could be predicted for future observations. We extracted transit predictions from our dynamical analysis of the posterior distribution. We found that accurate TTV predictions are very challenging due to the strong ambiguity in eccentricity versus dynamical planetary mass space (Lithwick et al. 2012). Due to the large multimodality of the TTVs, the error in transit predictions rapidly accumulates and is close to a few tens of days in 2023 and accumulates even more in future epochs. We tried to construct a joint N-body model (e.g., Trifonov et al. 2021a) from the available data and therefore predict future transits from fitting alone. However, the single-transit event and the relatively sparse RV data manifest in strong N-body model degeneracy in the posteriors, which is consistent with the TTV prediction from our stability analysis. The TTVs super period of the TIC 279401253 pair of exoplanets is of the order of the libration frequency of the resonance angles $\theta_{1,2}$, i.e., ∼20 yr. Our estimate shows that the semiamplitude within this secular timescale in many cases is of the order of tens of days. Thus, we could not give a meaningful prediction for the TTVs.

Nevertheless, the transiting planet is a prospective target for atmospheric investigation with the James Webb Space Telescope and ground-based extremely large telescopes, given its bright host star, $V \approx 11.9$ mag, the relatively short orbital period, and pronounced eccentricity. We plan to follow up this target with more RVs in an attempt to overcome the dynamical degeneracy and predict TTVs for future investigations.

4. Summary and Conclusions

We report the discovery of a warm pair of giant planets around the G-dwarf star TIC 279401253. The system is

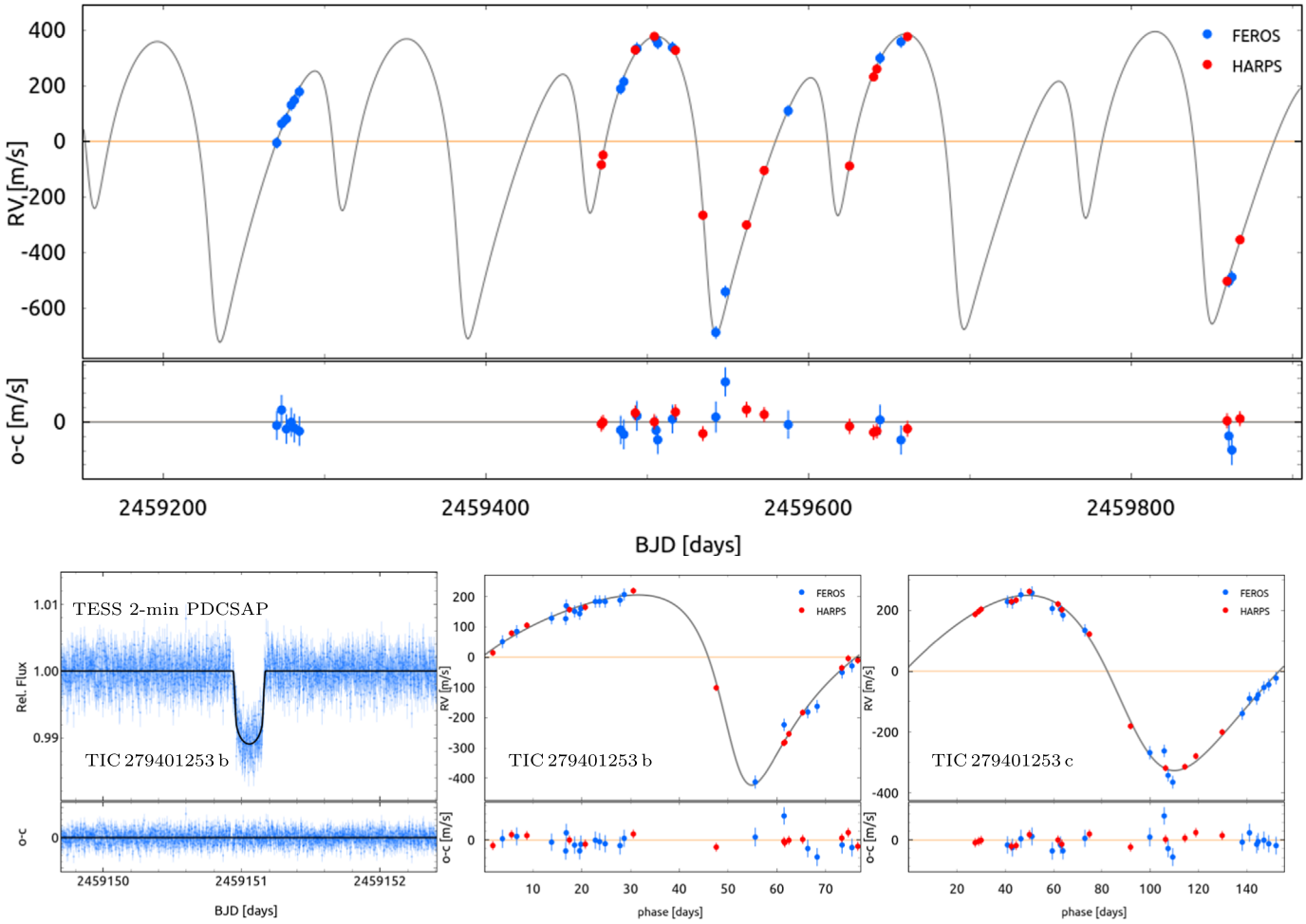

Figure 3. The top main panel shows the Doppler measurements from FEROS (blue) and HARPS (red) and the best two-planet model for these combined data. The left bottom panel shows the PDCSAP 2 minute TESS light curve of TIC 279401253 around the single-transit event recorded in Sector 31. The model curve shows the transit counterpart of the best-fit model applied jointly to the Doppler data obtained with FEROS and HARPS. The middle and right bottom panels show a phase-folded representation of the two planetary signals after the RV signal of the other companion was subtracted. The respective residuals are shown under each panel, accordingly.

revealed by TESS light-curve photometry and precise Doppler spectroscopy with FEROS and HARPS. Using the coadded HARPS spectra, we derived a stellar mass of $M_\star = 1.13^{+0.02}_{-0.03}$ $M_\odot$ and a stellar radius of $R_\star = 1.06^{+0.01}_{-0.01}$ $R_\odot$, among other physical and atmospheric stellar parameters. Using these stellar mass and radius estimates, we extensively analyzed the available data and constructed orbital posterior probability distributions. As a next step, we thoroughly analyzed the planetary system's dynamical architecture.

TIC 279401253 b is a transiting massive Jovian planet with a measured mass of $m_b = 6.14^{+0.39}_{-0.42}$ M_{jup}, and radius of $R_b = 1.00^{+0.04}_{-0.04}$ R_{jup}. Thus, the estimated density of TIC 279401253 b is $\rho_b = 8.2^{+1.1}_{-1.1}$ g cm^{-3}. Figure 5 shows the distribution of planets with measured radius and mass, color-coded for their density. The position of TIC 279401253 b on this plot places it among the densest planets discovered so far.

Based on the available RV data, we conclude that the outer planet, TIC 279401253 c, is similar to the inner super-Jovian planet with a minimum mass of $m_c = 8.02^{+0.18}_{-0.18}$ M_{jup}. The available TESS light curve from Sectors 4 and 31 do not have sufficient coverage to reveal whether TIC 279401253 c is transiting, but assuming its radius is consistent with that of TIC 279401253 b, then both planets in the system have high densities.

The warm pair of massive planets is found at the 2:1 period ratio commensurability with orbital periods of $P_b = 76.80^{+0.06}_{-0.06}$ days for the inner planet, and $P_c = 155.3^{+0.7}_{-0.7}$ days for the outer, respectively. We performed detailed *N*-body simulations of the posterior probability distributions to reveal the long-term stability and the overall dynamics of the TIC 279401253 system. We found that 73.4% of the posterior samples are stable for 1 Myr, and potentially beyond. The evolution of the apsidal alignment angle $\Delta\omega$, and the characteristic 2:1 MMR angles θ_1 and θ_2, exhibit libration about 0°. Thus, our numerical orbital analysis of the system unveiled that the massive pair of planets are deeply inside the first-order 2:1 MMR.

The TIC 279401253 system is strikingly similar to the 2:1 MMR pair orbiting HD 82943, as reported by Tan et al. (2013). Using a self-consistent dynamical fitting to the RV data of HD 82943, Tan et al. (2013) unveiled two massive Jovian planets whose orbital geometry, physical, and dynamical characteristics are analogous to those of TIC 279401253. For instance, Tan et al. (2013) found that the HD 82943 system is very likely inclined to $i = 19.5 \pm 5°$, which makes the dynamical masses of the HD 82943 planets consistent with

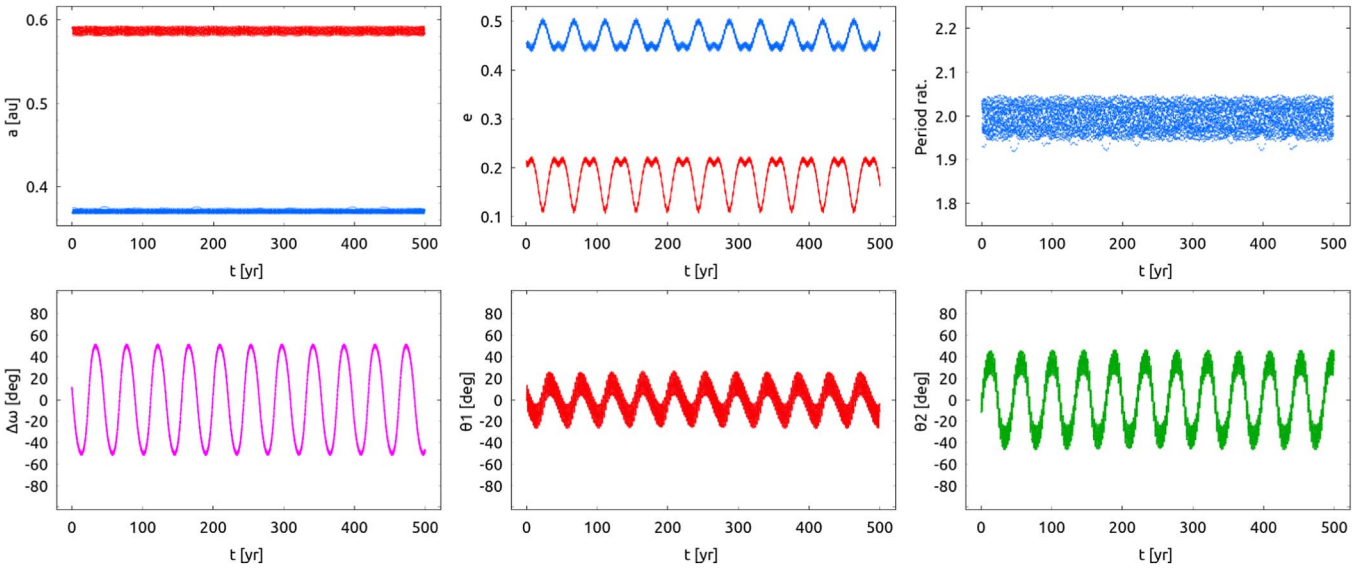

Figure 4. Orbital evolution of the TIC 279401253 system for a 500 yr extent for the best-fit solution. The top panels show the evolution of the semimajor axes $a_{b,c}$, the eccentricities $e_{b,c}$ (blue color indicates the inner, red color the outer planet), and planetary period ratio $P_{rat.}$. The bottom panels show the evolution of the apsidal alignment argument $\Delta\omega = \omega_c - \omega_b$ and the resonance angles θ_1 and θ_2, which librate around 0°, i.e., in a 2:1 MMR. See the text for details.

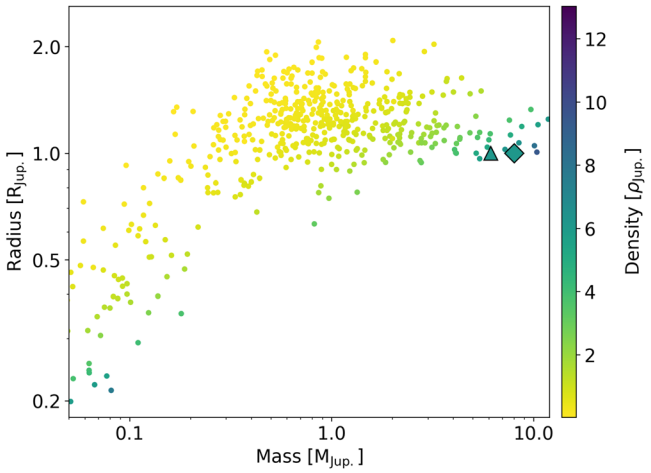

Figure 5. Mass–radius distribution of exoplanets, color-coded by their estimated mean density. TIC 279401253 b is marked with a triangle, among the densest warm Jovian planets found up-to-date. Assuming that TIC 279401253 c also has a Jupiter-like radius, its position is marked with a diamond-shaped sign.

those of TIC 279401253 b and c (see their Table 6). Furthermore, the orbital geometry and dynamical evolution of the two systems inside the 2:1 MMR exhibit practically the same pattern (see our Figure 4, and, e.g., Figure 7 in Tan et al. 2013).

It is plausible to assume that both systems have undergone a common formation and orbital evolution history. Such massive planet pairs are likely assembled during convergent migration in massive primordial circumstellar disks (e.g., Lee & Peale 2002; Kley & Nelson 2012). For instance, such massive planets must have gone through a slow type II migration. Given the almost equal mass ratio and large osculating eccentricities, it suggests that the planets were locked in the 2:1 MMR with initially nonzero eccentricity (see Lee 2004). This is intriguing since planet–disk interactions tend to damp the eccentricity. Nonetheless, Papaloizou et al. (2001) showed that planet–disk interactions could pump the eccentricity of very massive Jovians up to ≈0.25, which is a plausible mechanism for eccentricity excitation in the disk. Alternatively, the migration of massive planets through the disk creates wide gaps, and this leads to excitation of the eccentricities in the disk (see, e.g., Goldreich & Tremaine 1980; Goldreich & Sari 2003).

Therefore, the TIC 279401253 and HD 82943 systems and their dynamical similarities are crucial forensic evidence for planetary formation mechanisms.

This research has made use of the Exoplanet Follow-up Observation Program website, which is operated by the California Institute of Technology, under contract with the National Aeronautics and Space Administration under the Exoplanet Exploration Program. Funding for the TESS mission is provided by NASA's Science Mission directorate. This paper includes data collected by the TESS mission, which are publicly available from the Mikulski Archive for Space Telescopes (MAST). Resources supporting this work were provided by the NASA High-End Computing (HEC) Program through the NASA Advanced Supercomputing (NAS) Division at Ames Research Center for the production of the SPOC data products. V.B., D.A., D.S., M.M., and T.T. acknowledge support by the BNSF program "VIHREN-2021" project No. KP-06-DV-5/15.12.2021. T.T. acknowledges support by the DFG Research Unit FOR 2544 "Blue Planets around Red Stars" project No. KU 3625/2-1. A.J., R.B., M.H. and F.R. acknowledge support from ANID—Millennium Science Initiative—ICN12_009. D.D. acknowledges support from the NASA Exoplanet Research Program grant 18-2XRP18_2-0136. A.J. acknowledges additional support from FONDECYT project 1210718. R.B. acknowledges support from FONDECYT project 11200751. This work was also funded by the Data Observatory Foundation. We thank Yair Judkovsky for useful discussion on the TTV analysis. We thank the anonymous reviewer for very helpful comments and suggestions.

Appendix

In this Appendix, Figure A1 shows the posterior probability distribution of the joint Doppler and TESS photometry modeling with `Exo-Striker`, in Tables A1 and A2 we list the spectroscopically derived RVs and activity index time-series from FEROS, and HARPS, respectively.

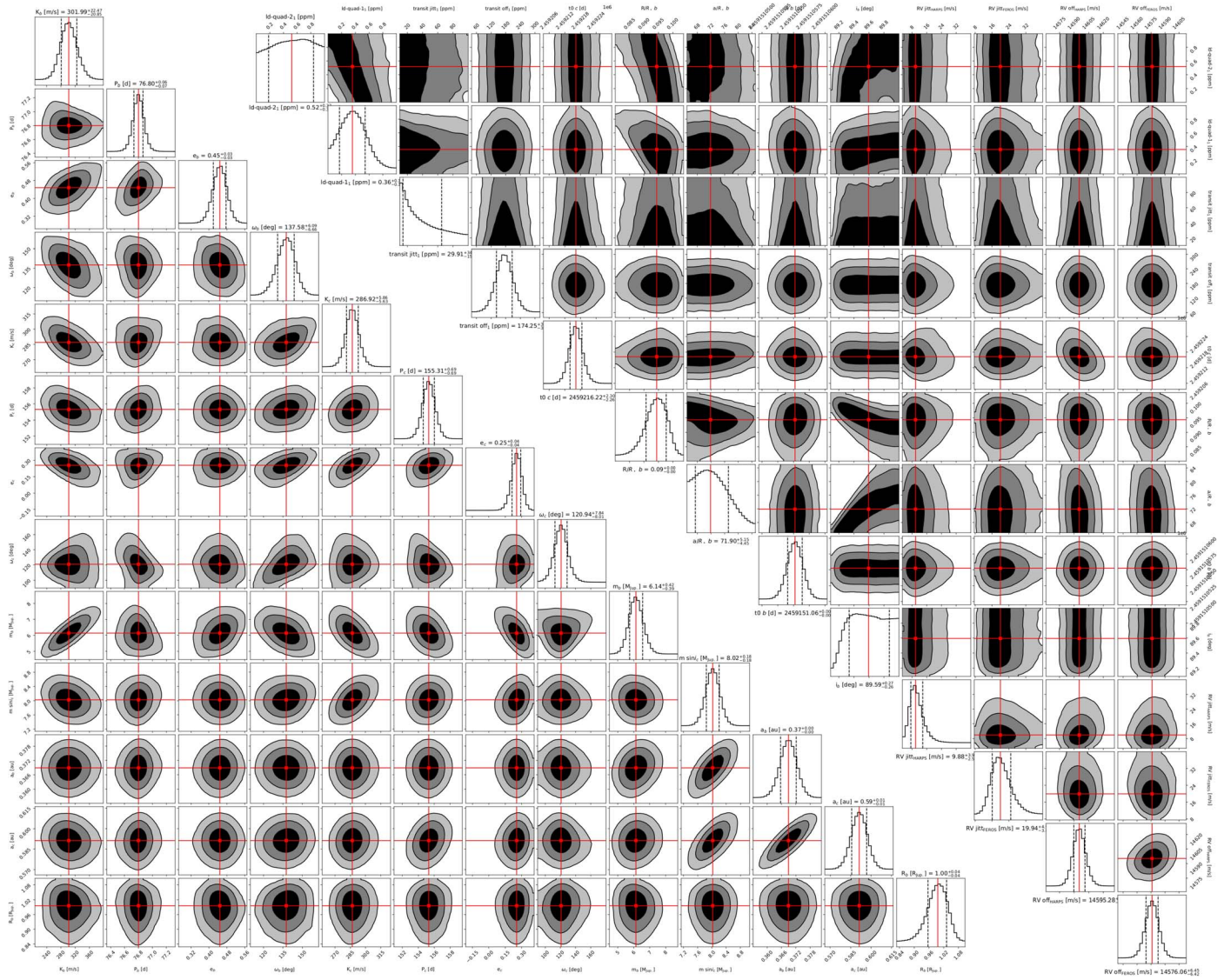

Figure A1. Nested Sampling posteriors the two-planet system TIC 279401253.

Table A1
FEROS Doppler and Activity Measurements of TIC279401253

Epoch (JD)	RV (m s^{-1})	σ_{RV} (m s^{-1})	BIS (m s^{-1})	σ_{BIS} (m s^{-1})
2,459,270.543	14574.3	7.6	7.0	10.0
2,459,273.545	14643.0	9.6	−23.0	12.0
2,459,276.533	14660.3	8.8	−29.0	12.0
2,459,279.508	14710.4	8.2	−5.0	11.0
2,459,281.511	14727.6	7.4	13.0	10.0
2,459,284.548	14758.1	8.8	−16.0	12.0
2,459,483.716	14768.8	7.4	20.0	10.0
2,459,485.732	14794.3	9.2	5.0	12.0
2,459,493.858	14913.7	9.2	9.0	12.0
2,459,505.706	14946.1	7.4	−26.0	10.0
2,459,506.738	14932.5	7.3	−14.0	10.0
2,459,515.848	14917.1	7.3	22.0	10.0
2,459,542.720	13892.6	11.1	15.0	14.0
2,459,548.660	14039.0	7.8	−6.0	11.0
2,459,587.626	14689.6	7.2	0.0	10.0
2,459,644.531	14878.9	9.8	20.0	13.0
2,459,657.509	14937.9	8.2	−10.0	11.0
2,459,860.777	14075.8	8.0	13.0	11.0
2,459,862.698	14091.6	9.4	35.0	12.0

Table A2
HARPS-DRS Doppler and Activity Measurements of TIC279401253

Epoch (JD)	RV (m s^{-1})	σ_{RV} (m s^{-1})	FWHM (m s^{-1})	BIS (m s^{-1})	Contrast
2,459,471.788	14509.7	2.8	7606.6	−1.9	45.9
2,459,472.833	14544.4	2.9	7626.7	5.9	45.8
2,459,492.795	14922.7	3.3	7608.6	0.4	45.8
2,459,504.640	14971.6	3.5	7594.8	−23.0	45.8
2,459,517.727	14921.4	2.6	7578.6	−0.4	45.9
2,459,534.741	14328.6	2.2	7578.3	9.9	45.9
2,459,561.786	14293.7	4.1	7591.9	11.7	46.1
2,459,572.746	14489.2	2.6	7579.1	31.5	46.3
2,459,625.614	14505.3	3.5	7523.2	−39.3	45.5
2,459,640.574	14826.0	3.0	7584.4	−19.9	46.1
2,459,642.559	14854.1	2.6	7595.5	4.9	46.0
2,459,661.514	14970.8	4.4	7623.1	−34.9	46.2
2,459,859.724	14091.4	3.2	7617.2	9.8	45.8
2,459,867.729	14240.4	2.6	7592.3	−5.3	46.0

ORCID iDs

Vladimir Bozhilov https://orcid.org/0000-0002-3117-7197
Desislava Antonova https://orcid.org/0000-0003-1507-7230
Melissa J. Hobson https://orcid.org/0000-0002-5945-7975
Rafael Brahm https://orcid.org/0000-0002-9158-7315
Andrés Jordán https://orcid.org/0000-0002-5389-3944
Thomas Henning https://orcid.org/0000-0002-1493-300X
Jan Eberhardt https://orcid.org/0000-0003-3130-2768
Felipe I. Rojas https://orcid.org/0000-0003-3047-6272
Konstantin Batygin https://orcid.org/0000-0002-7094-7908
Pascal Torres-Miranda https://orcid.org/0000-0003-0974-210X
Keivan G. Stassun https://orcid.org/0000-0002-3481-9052
Sarah C. Millholland https://orcid.org/0000-0003-3130-2282
Denitza Stoeva https://orcid.org/0000-0001-6277-9644
Milen Minev https://orcid.org/0000-0002-5702-5095
Nestor Espinoza https://orcid.org/0000-0001-9513-1449
George R. Ricker https://orcid.org/0000-0003-2058-6662
David W. Latham https://orcid.org/0000-0001-9911-7388
Diana Dragomir https://orcid.org/0000-0003-2313-467X
Michelle Kunimoto https://orcid.org/0000-0001-9269-8060
Jon M. Jenkins https://orcid.org/0000-0002-4715-9460
Eric B. Ting https://orcid.org/0000-0002-8219-9505
Sara Seager https://orcid.org/0000-0002-6892-6948
Joshua N. Winn https://orcid.org/0000-0002-4265-047X
Jesus Noel Villasenor https://orcid.org/0000-0002-4625-8264
Luke G. Bouma https://orcid.org/0000-0002-0514-5538
Jennifer Medina https://orcid.org/0000-0002-3284-4713
Trifon Trifonov https://orcid.org/0000-0002-0236-775X

References

Baluev, R. V. 2008, MNRAS, 385, 1279
Baluev, R. V. 2009, MNRAS, 393, 969
Borucki, W. J., Koch, D., Basri, G., et al. 2010, Sci, 327, 977
Brahm, R., Hartman, J. D., Jordán, A., et al. 2018, AJ, 155, 112
Brahm, R., Jordán, A., & Espinoza, N. 2017a, PASP, 129, 034002
Brahm, R., Jordán, A., Hartman, J., & Bakos, G. 2017b, MNRAS, 467, 971
Brahm, R., Nielsen, L. D., Wittenmyer, R. A., et al. 2020, AJ, 160, 235
Bressan, A., Marigo, P., Girardi, L., et al. 2012, MNRAS, 427, 127
Duncan, M. J., Levison, H. F., & Lee, M. H. 1998, AJ, 116, 2067
Espinoza, N., Brahm, R., Henning, T., et al. 2020, MNRAS, 491, 2982
Gaia Collaboration, Brown, A. G. A., Vallenari, A., et al. 2021, A&A, 649, A1
Goldreich, P., & Sari, R. 2003, ApJ, 585, 1024
Goldreich, P., & Tremaine, S. 1980, ApJ, 241, 425
Jenkins, J. M., Twicken, J. D., McCauliff, S., et al. 2016, Proc. SPIE, 9913, 99133E
Jordán, A., Brahm, R., Espinoza, N., et al. 2020, AJ, 159, 145
Kaufer, A., Stahl, O., Tubbesing, S., et al. 1999, Msngr, 95, 8
Kley, W., & Nelson, R. P. 2012, ARA&A, 50, 211
Lee, M. H. 2004, ApJ, 611, 517
Lee, M. H., & Peale, S. J. 2002, ApJ, 567, 596
Lithwick, Y., Xie, J., & Wu, Y. 2012, ApJ, 761, 122
Mayor, M., Pepe, F., Queloz, D., et al. 2003, Msngr, 114, 20
Nelder, J. A., & Mead, R. 1965, CompJ, 7, 308
Papaloizou, J. C. B., Nelson, R. P., & Masset, F. 2001, A&A, 366, 263
Pepe, F., Mayor, M., Rupprecht, G., et al. 2002, Msngr, 110, 9
Press, W. H., Teukolsky, S. A., Vetterling, W. T., & Flannery, B. P. 1992, Numerical Recipes in FORTRAN. The Art of Scientific Computing (Cambridge: Cambridge Univ. Press)
Queloz, D., Henry, G. W., Sivan, J. P., et al. 2001, A&A, 379, 279
Ricker, G. R., Winn, J. N., Vanderspek, R., et al. 2015, JATIS, 1, 014003
Sandford, E., Espinoza, N., Brahm, R., & Jordán, A. 2019, MNRAS, 489, 3149
Schlecker, M., Kossakowski, D., Brahm, R., et al. 2020, AJ, 160, 275
Skilling, J. 2004, in AIP Conf. Ser. 735, Bayesian Inference and Maximum Entropy Methods in Science and Engineering, ed. R. Fischer, R. Preuss, & U. V. Toussaint (Melville, NY: AIP), 395
Smith, J. C., Stumpe, M. C., Van Cleve, J. E., et al. 2012, PASP, 124, 1000
Speagle, J. S. 2020, MNRAS, 493, 3132
Stumpe, M. C., Smith, J. C., Van Cleve, J. E., et al. 2012, PASP, 124, 985
Tan, X., Payne, M. J., Lee, M. H., et al. 2013, ApJ, 777, 101
Trifonov, T. 2019, The Exo-Striker: Transit and Radial Velocity Interactive Fitting Tool for Orbital Analysis and N-body Simulations, Astrophysics Source Code Library, ascl:1906.004
Trifonov, T., Brahm, R., Espinoza, N., et al. 2021a, AJ, 162, 283
Trifonov, T., Caballero, J. A., Morales, J. C., et al. 2021b, Sci, 371, 1038